APPLIED GEOPHYSICS, Vol.21, No.4 (December 2024), P. 1–17, 12 Figures.
DOI:10.1007/s11770-024-1128-1

Earthquake detection probabilities and completeness magnitude in the northern margin of the Ordos Block

Zhang Fan[1,3] Yang Xiao-Zhong[2]*, and Cui Feng-Zhi[3]

Abstract: The assessment of the completeness of earthquake catalogs is a prerequisite for studying the patterns of seismic activity. In traditional approaches, the minimum magnitude of completeness (M_C) is employed to evaluate catalog completeness, with events below M_C being discarded, leading to the underutilization of the data. Detection probability is a more detailed measure of the catalog's completeness than M_C; its use results in better model compatibility with data in seismic activity modeling and allows for more comprehensive utilization of seismic observation data across temporal, spatial, and magnitude dimensions. Using the magnitude–rank method and Maximum Curvature (MAXC) methods, we analyzed temporal variations in earthquake catalog completeness, finding that M_C stabilized after 2010, which closely coincides with improvements in monitoring capabilities and the densification of seismic networks. Employing the probability-based magnitude of completeness (PMC) and entire magnitude range (EMR) methods, grounded in distinct foundational assumptions and computational principles, we analyzed the 2010–2023 earthquake catalog for the northern margin of the Ordos Block, aiming to assess the detection probability of earthquakes and the completeness of the earthquake catalog. The PMC method yielded the detection probability distribution for 76 stations in the distance–magnitude space. A scoring metric was designed based on station detection capabilities for small earthquakes in the near field. From the detection probabilities of stations, we inferred detection probabilities of the network for different magnitude ranges and mapped the spatial distribution of the probability-based completeness magnitude. In the EMR method, we employed a segmented model fitted to the observed data to determine the detection probability and completeness magnitude for every grid point in the study region. We discussed the sample dependency and low-magnitude failure phenomena of the PMC method, noting the potential overestimation of detection probabilities for lower magnitudes and the underestimation of M_C in areas with weaker monitoring capabilities. The results obtained via the two methods support these hypotheses. The assessment results indicate better monitoring capabilities on the eastern side of the study area but worse on the northwest side. The spatial distribution of network monitoring capabilities is uneven, correlating with the distribution of stations and showing significant differences in detection capabilities among different stations. The truncation effects of data and station selection affected the evaluation results at the edges of the study area. Overall, both methods yielded detailed descriptions of the earthquake catalog, but careful selection of calculation parameters or adjustments based on the strengths of different methods is necessary to correct potential biases.
Keywords: magnitude of completeness; northern margin of the Ordos Block; PMC method; EMR method; earthquake detection probability

Introduction

Statistical seismology models the probabilistic distribution of seismic activity, bridging the gap between physical and statistical models. Relevant models include the G–R model (Gutenberg and Richter, 1944; Ram et al., 2022) and the ETAS model (Zhuang, 2011; Bi et

Manuscript received by the Editor March 2, 2024; revised manuscript received July 12, 2024.
This research project is funded by Director Fund of the Inner Mongolia Autonomous Region Seismological Bureau (No. 2023GG02, 2023MS05) and the Inner Mongolia Natural Science Foundation (No. 2024MS04021)
1. College of Control and Computer Engineering, North China Electric Power University, Beijing 102206, China
2. College of Mathematics and Physics, North China Electric Power University, Beijing 102206, China
3. Inner Mongolia Autonomous Region Seismological Bureau, Hohhot 010051, China
*Corresponding author: Yang Xiao-Zhong (Email: yxiaozh@ncepu.edu.cn).

al., 2023). The effectiveness of these models is affected by the quantity and quality of seismic data, making the efficient use of limited earthquake data an important research topic. The magnitude of completeness (M_C), the lowest magnitude that can be recorded with 100% certainty, is typically used to assess the completeness of earthquake catalogs. Most M_C estimation methods are based on the assumptions of the G–R model, where M_C is defined as the smallest magnitude at which the cumulative frequency of magnitude distribution deviates from the G–R model (Zúñiga and Wyss, 1995). Several evaluation methods based on the G–R model have been developed (Wiemer and Wyss, 2000; Cao and Gao, 2002; Woessner and Wiemer, 2005), with some of them relying less on the assumptions of the G–R model (Rydelek and Sacks, 1989; Kagan, 2003; Amorèse, 2007). The noise spectra of seismic stations can also be used to assess M_C (Gomberg, 1991; Kværna and Ringdal, 1999). Waveform forward modeling techniques used for evaluating the accuracy of seismic source localization (D'Alessandro et al., 2011) can also be used to estimate data completeness. Some methods, such as the probability-based magnitude of completeness (PMC) method (Schorlemmer and Woessner, 2008; Li and Huang, 2014; Jiang et al., 2015; Schorlemmer et al., 2018) and the Bayesian magnitude of completeness (BMC) method (Mignan et al., 2011, 2013), combine information from earthquake catalogs and stations. The PMC method does not depend on the G–R model and uses only actual observational data, including phase data and station information. The BMC method optimizes spatial resolution through the integration of prior information on station density with local observations. The hierarchical Bayesian model, developed based on the BMC method, exhibits higher accuracy than the BMC method (Feng et al., 2022). The generalized gamma function model can be used for the estimation of earthquake catalog completeness, detection probability, and *b*-values, enhancing the accuracy of *b*-value estimation (Martinsson and Jonsson, 2018). The normalized distance method (Lombardi, 2021) combines maximum likelihood estimation, goodness-of-fit tests, and bootstrapping to provide more accurate estimates of M_C and *b*-values. Leptokaropoulos et al. (2018) discussed the impact of magnitude uncertainty on the estimation of earthquake catalog parameters.

The overestimation of M_C can lead to the underutilization of earthquake catalogs, whereas underestimation can introduce inaccuracies in the estimates of model parameters. Earthquake catalogs are inherently heterogeneous and complex datasets affected by seismic network limitations and spatiotemporal variations in earthquake activity (Mignan and Woessner, 2012). Earlier earthquake catalogs tend to have lower completeness, whereas recent catalogs have higher completeness owing to the advancement of seismic networks. To incorporate both older and newer data, a higher M_C threshold might be necessary, but this often results in the discarding of valuable low-magnitude information from the more recent, complete data. Conversely, opting for a lower M_C necessitates the reduction of the time span of the earthquake catalog, and a similar dilemma exists spatially. Consequently, researchers are often compelled to adopt overly conservative M_C estimation methods (Mizrahi et al., 2021). After large earthquakes, because of the strong temporal clustering of seismic activity, monitoring networks can only capture a subset of events during periods of high activity (Kagan, 2004), leading to short-term aftershock incompleteness (Hainzl, 2022). The incorporation of variable M_C or detection probability as parameters in earthquake models can account for the heterogeneity in M_C, extending the range of seismic data used for model parameter estimation and improving model fitting (Omi et al., 2014; Hainzl, 2016).

Various researchers have compared catalog evaluation methods in terms of reliability. Mignan (2012) examined how the shape of the frequency–magnitude distribution (FMD) impacts the reliability of results. Mignan and Woessner (2012) compared the effectiveness of six catalog evaluation methods, and Huang et al. (2016) conducted numerical tests on five methods, revealing that the entire magnitude range (EMR) method is stable but generally underestimates M_C. Zhou et al. (2018) analyzed the stability and reliability of five methods under low event numbers and spatiotemporal heterogeneity. Pavlenko and Zavyalov (2022) compared the effectiveness of six methods using synthetic catalogs, exploring the effects of sample size and initial magnitude distribution shape on estimation results. Gong et al. (2024) employed synthetic data to assess the stability and accuracy of eight methods for estimating M_C. Whereas previous studies have extensively discussed M_C estimation, the evaluation of detection probability has received less attention.

The PMC method estimates the catalog completeness of seismic networks based on the detection probabilities of seismic stations. In the EMR method (Woessner and Wiemer, 2005), a model that incorporates detection

probability is fitted to the FMD across the entire magnitude range. Although PMC and EMR methods are based on different prior assumptions and computational principles, both can estimate earthquake detection probabilities and completeness magnitudes. Herein, we applied both methods to earthquake observation data from the northern Ordos Block margin between 2010 and 2023 to evaluate both the detection probabilities and the completeness of the earthquake catalog. Through a comparative analysis of the results, we assessed the applicability and accuracy of the two methods and elaborated on the quality of the earthquake catalog for the study area. Overall, the present study contributes to the understanding of detection probability estimation.

Data Overview

The northern margin of the Ordos Block (38°–42°N, 104°–116°E), located at the junction of several active tectonic blocks, was selected as the study area. This region, characterized by a history of significant earthquakes and numerous active faults since the Holocene epoch, presents a considerable risk of future seismic events (Xu et al., 2017). It stands out as a primary zone of strong seismic activity in Northern China (Gao et al., 2016). We utilized the earthquake catalog of the China Seismic Network, which covers the period from 1965 to 2023 and contains a total of 48805 earthquake records in local magnitude M_L (further used as a default magnitude unit). We employed the magnitude–rank method and the Maximum Curvature (MAXC) method (Wiemer and Wyss, 2000) to qualitatively and quantitatively analyze the temporal changes in the completeness of the earthquake catalog. In the magnitude–rank method (Figure 1(a)), earthquake events are sorted in chronological order to observe the distribution of earthquake density in both time and magnitude (Bi et al., 2023). Areas with high earthquake density correspond to M_C; importantly, this method can exclude the impact of "clustered events" on the results (Jiang and Wu, 2011). For quantitative analysis, the MAXC method was used to evaluate the temporal characteristics of M_C in the study area with a window length of 500 events (Figure 1(b)).

Figures 1(a) and 1(b) reveal a stepwise decrease in M_C for the study area between 1965 and 2023, stabilizing after 2010. Based on these trends, we divided the earthquake catalog into three distinct periods. The first period, spanning 1965 to 1996, shows a relatively stable M_C that fluctuates around magnitude 2, with a brief

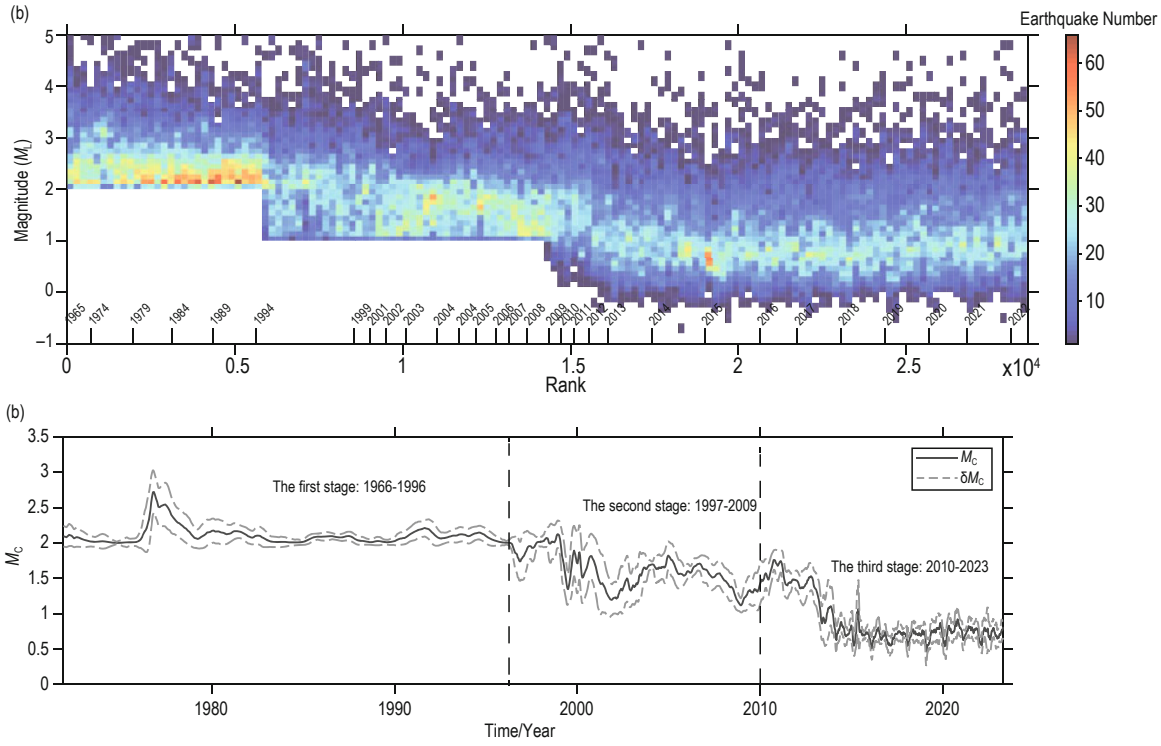

Figure 1. Temporal variation in M_C in the study area in 1976–2023. (a) Magnitude–Rank chart; (b) MAXC results.

increase to approximately 4.0 after the 1976 earthquake, followed by a gradual recovery to around 2.0 by 1987. The second period, from 1997 to 2009, coincides with the implementation of the "China Digital Seismograph Network" (Liu et al., 2008) and exhibits M_C values fluctuating between 1.0 and 2.0. Lastly, the third period, covering 2010–2023, shows a significant decline in M_C followed by stabilization between 0.5 and 1.5, coinciding with the implementation of the "15th Five-Year Plan" for the digital observation platform by the China Earthquake Administration. Importantly, Figure 1(a) reveals a wealth of data below the determined M_C, highlighting the substantial variation in monitoring capabilities over time. The use of a fixed M_C would inevitably lead to the exclusion of a significant portion of data across temporal, spatial, or magnitude dimensions.

The dataset utilized for the comparative analysis of the PMC and EMR methods encompasses earthquake observation data from 2010 to 2023, including a catalog of 26,057 earthquakes and observation reports from 76 permanent seismic stations. Figure 2 shows the spatial distribution of earthquakes and seismic stations in the study area (Figure 2(a)), the magnitude–frequency and cumulative frequency distributions (Figure 2(b)), and the annual earthquake counts (Figure 2(c)). The spatial distribution of earthquakes in the study area is heterogeneous: earthquakes are primarily concentrated within the rift zones along the periphery of the Ordos Block, with lower seismicity levels observed in the interior part of the block and along its northern boundary. The spatial distribution of seismic stations is also non-uniform, with a higher station density in the eastern part of the study region.

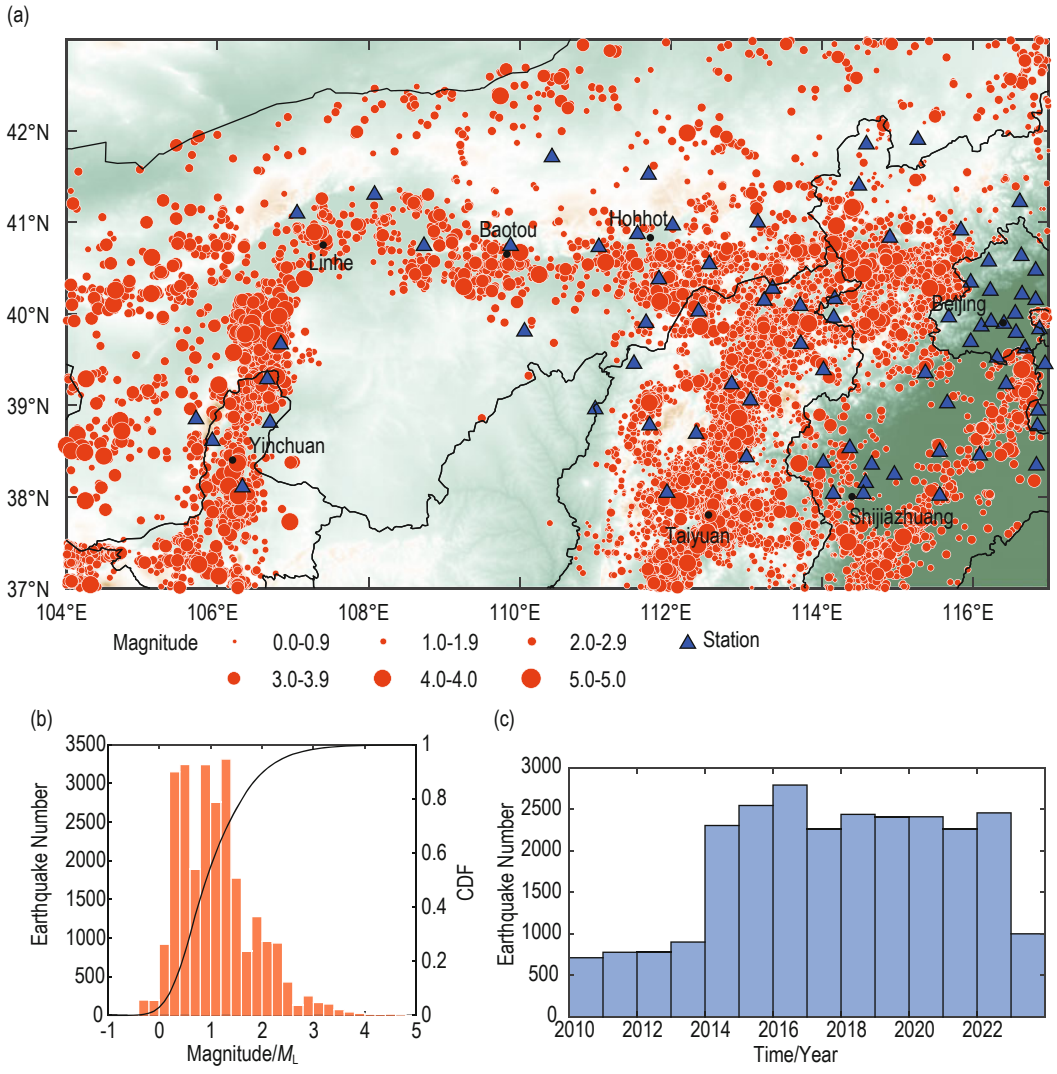

Figure 2. Data Overview

(a) Earthquake epicenters and seismic stations; (b) magnitude–frequency distribution and CDF; (c) annual earthquake counts.

Method

PMC

In the PMC method, first, the distribution of detection probability is determined for each station within a two-dimensional parameter space defined by magnitude and distance. Based on these individual station probabilities, we calculated the probability that each grid point in the spatial domain is simultaneously detected by a specific number of stations (set to 4 based on the actual network configuration). This yielded a detection probability distribution map for the network. By setting a detection probability threshold Q, we defined the smallest magnitude that meets this threshold as the probability-based magnitude of completeness (denoted as M_P in this paper).

In the first step, the probability of detection for each station was calculated (Schorlemmer and Woessner, 2008). Earthquake events recorded by the network were plotted in a two-dimensional coordinate system of magnitude (M) and epicentral distance (L). Distance L and magnitude M were then unified into a single magnitude unit using a calibration function specific to the China region. In the unified magnitude–magnitude space, events within a Euclidean distance of 0.1 were considered (if the sample size was less than 10, the range was expanded to at least 10 samples). The number of events detected ($N+$) and not detected ($N-$) by the station under consideration were then used to calculate detection probability $P_D(M, L)$ for the station at (M, L) using Equation (1):

$$P_D(M,L) = \frac{N_+}{N_+ + N_-}. \quad (1)$$

We smoothed the probability distribution of stations through simple physical constraints. (1) At the same distance, the detection probability should not decrease with the increase in magnitude. (2) For the same magnitude, the detection probability should not decrease with the decrease in distance. This smoothing method was employed to address data sparsity while adhering to physical principles.

In the second step, the detection probability for the entire network was calculated for earthquakes of different magnitudes at each grid point, referred to as the synthetic detection probability (P_E). It is the joint probability of multiple stations simultaneously recording an event. The probability of an earthquake being detected by at least 4 stations was calculated by subtracting the probabilities of detection by fewer than 4 stations from 1, as expressed in Equation (2):

$$P_E = 1 - \sum_{i=0}^{3} P_E^i. \quad (2)$$

Here, P_E^i represents the probability that an earthquake at a certain grid point is detected by exactly i stations.

The completeness magnitude, M_P, is defined as the minimum magnitude M at which P_E reaches threshold Q (Equation 3).

$$M_P = \min_{M \in M} M \mid P_E(M) = 1 - Q. \quad (3)$$

Q is the threshold level for earthquakes to be missed, set at 0.001.

The average spacing between stations in the study area exceeds 50 km. Because of the limited accuracy of the data on the depth of earthquake sources in the catalog, we did not consider the effect of source depth (an average depth of 15 km was assumed). The statistical range for station detection probability was set from epicentral distance 0–400 km and magnitude 0–5.

EMR

The EMR method (Woessner and Wiemer, 2005) models the entire range of the FMD. The high-magnitude segment (which conforms to the Gutenberg–Richter relationship) is described by a simple power-law function, expressed as $\log N(M) = a - bM$, where $N(M)$ represents the frequency of earthquakes with magnitude greater than or equal to M; a and b are fitting parameters; and M is the magnitude.

For the incomplete part below the M_C, the detection probability is described using a one-sided normal distribution, denoted by q (Equation (4)). Initially, the MAXC method is used to estimate M_C. Then, near this estimated value, a segmented function is fitted using maximum likelihood estimation to obtain estimates of parameters μ and σ. The fit of the segmented function is evaluated using the Kolmogorov–Smirnov test at a significance level of 0.05 (Conover, 1999). Bootstrap resampling is used to compute a 95% confidence interval, assessing the uncertainty of M_C.

$$q(M \mid \mu\sigma) = \begin{cases} \frac{1}{\sigma\sqrt{2\pi}} \int_{\infty}^{M_c} \exp\left(-\frac{(M-\mu)^2}{2\sigma^2}\right) dM, M < M_c. \\ 1, M \geqslant M_c \end{cases} \quad (4)$$

Here, μ represents the magnitude at which 50% of earthquakes are detected, and σ is the corresponding

standard deviation. A higher σ value indicates a rapid decrease in the network's detection capability. Above the M_C, the detection probability of earthquakes is 1. Figure 3 shows the results for a subset of data from the study area (1000 earthquakes). Figure 3(a) shows the results on a logarithmic scale, with M_C estimated at 1.5. It displays the theoretical FMD (circles, based on the EMR model), theoretical cumulative FMD (CFMD; dashed line, based on the G–R model), observed FMD (diamonds), and observed CFMD (triangles). The segmented model of the EMR method fits the data well on both sides of M_C. Figure 3(b) shows the likelihood as a function of magnitude, and Figure 3(c) exhibits the probability of detection as a function of magnitude, derived from the ratio of the theoretical FMD according to the EMR model and the G–R model across different magnitude bins. The positions of points deviating from the horizontal line correspond to M_C.

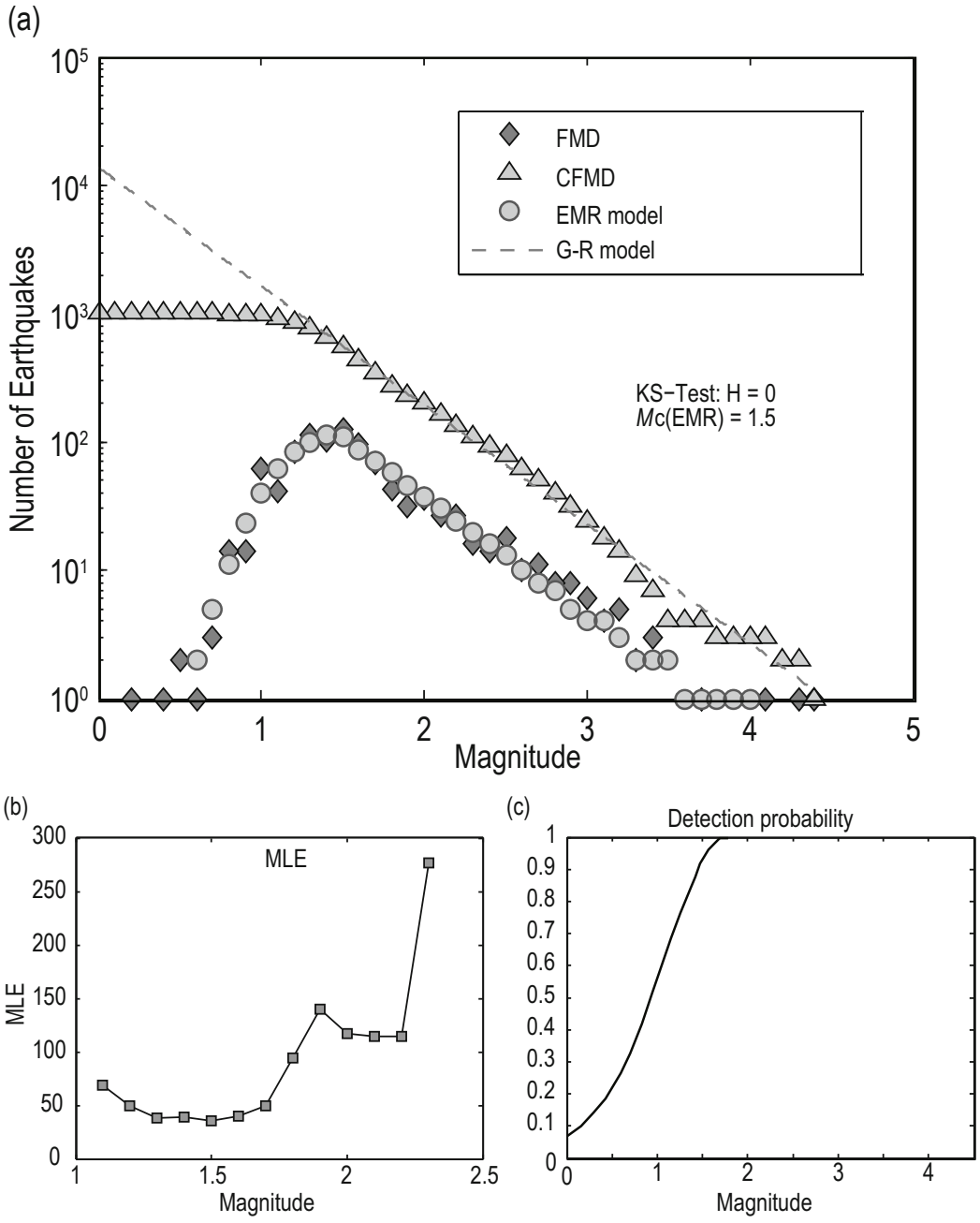

Figure 3. Example EMR results
(a) FMD and CFMD (Fitting results of the G–R and EMR models); (b) likelihood (MLE) as a function of magnitude; (c) probability of detection as a function of magnitude.

Result

Station-Wise Detection Probability

To assess the detection probability for 76 seismic stations using the PMC method, we used the average detection probability within 200 km for earthquakes of magnitude 3 or less as the evaluation metric. This approach is simpler than that employed by Wang et al. (2017) because it uses a single value to represent the detection capabilities of a station, which provides some information about the detection probability. Stations with better recording capabilities for nearby earthquakes have larger areas where the detection probability reaches 1, resulting in a higher average detection probability. Therefore, a single metric can be used to effectively compare the earthquake detection capabilities of stations in the study area. Herein, "detection capability" primarily describes a station's ability to record earthquakes, corresponding to the detection probability of a staion. At the same time, "monitoring capability" mainly describes the seismic network's ability to record earthquakes within a spatiotemporal area, corresponding to the detection probability and completeness magnitude of the network.

Figure 4 shows the distribution and frequency of station scores. In Figure 5, stations are categorized into three categories (good, moderate, and poor), showing examples of their recording capabilities through original data plots and detection probability distribution plots. In the original data plots, red and green dots represent earthquakes not recorded and recorded in the station's catalog, respectively. For example, the JIZ station scores 0.13, indicating that it hardly recorded earthquakes below magnitude 2 within 100 km and only detected earthquakes above magnitude 2.5 within 50 km. The XIJ station scores 0.35, showing that it detected earthquakes above magnitude 1 within 50 km and earthquakes above magnitude 3 within 150 km. The SHZ station scores 0.65, indicating that it detected earthquakes below magnitude 0.5 within 50 km, earthquakes above magnitude 1.5 within 100 km, and earthquakes above magnitude 3 within 300 km. Owing to data truncation, some stations at the edges of the study area have lower scores, particularly stations on the southeast side.

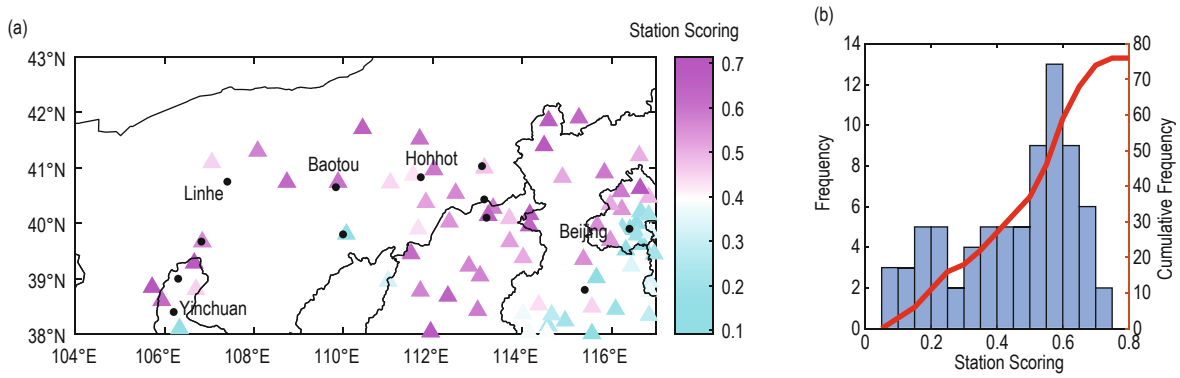

Figure 4. Spatial distribution and frequency plot of station scores: (a) station map with scores; (b) cumulative and noncumulative frequency distributions of station scorings.

Seismic signals recorded by a station should be positively correlated with magnitude and negatively correlated with distance. The detection probability should also follow these patterns and exhibit continuous variation. However, some stations exhibit different tendencies in their detection probability plots (Figure 6). For instance, the detection probability of the NIW station for low-magnitude events does not decrease with distance (Figure 6(a)). This anomaly was attributed to the incompleteness of the earthquake catalog for low-magnitude events in the seismic network, resulting in the underestimation of the denominator when calculating detection probability, thus resulting in the overestimation of the latter Equation (1). Schorlemmer et al. (2018) discussed similar situations. The detection probability of the NIW station rapidly drops to near zero beyond 150 km, indicating the underutilization of this station for the detection of more distant earthquakes within the study area. The BTO station shows a distinct step-like pattern around magnitude 1, caused by insufficient data for low-magnitude events.

Earthquake Detection Probability and Magnitude of Completeness

When using the PMC method, after obtaining the detection probability for each station, the synthetic detection probability formula (Equation (2)) was applied to derive the synthetic detection probability, P_E, for different magnitude bins. This P_E represents the detection probability of the seismic network and is denoted as P(PMC). For the EMR method, a spatial grid with a resolution of 0.1° × 0.1° was employed. A circular area with a radius of 100 km centered on each grid point was used to define the earthquake event selection zone. A minimum earthquake count threshold of 50 events was used in the analysis. To evaluate δM_C, 100 bootstrap resampling iterations were performed, ultimately yielding the spatial distributions of both the completeness magnitude (M_C(EMR)) and the detection probability (P(EMR)) at different magnitude levels. We then plotted the detection probability distributions for both methods at magnitudes 0.3,0.5,0.8,1.0,1.5 and 2.0 (first two columns in Figure 7), along with the differences in detection probabilities between the two methods (third column in Figure 7).

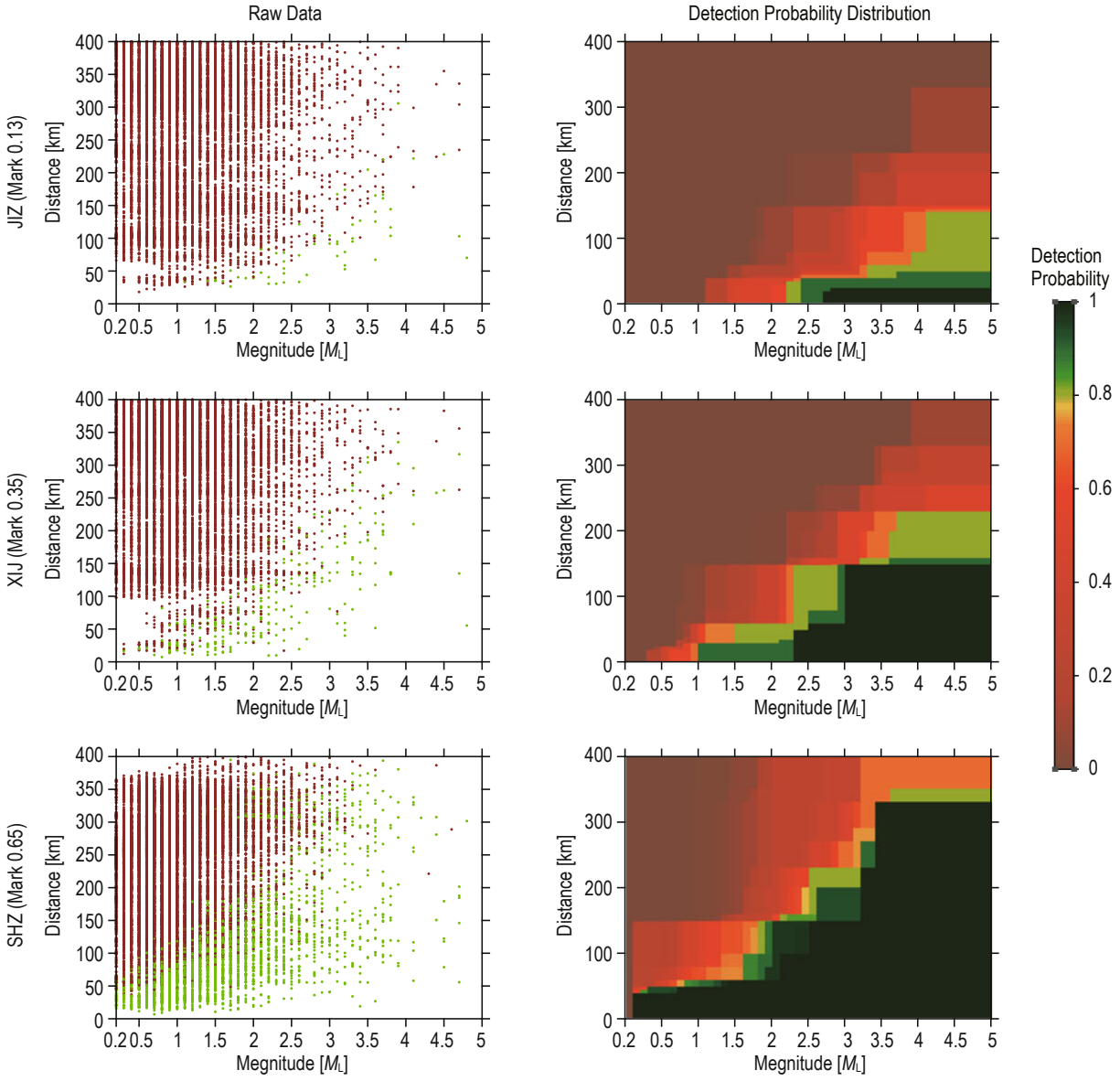

Figure 5 Station-wise detection probabilities for three score ranges.
The graph presents data and detection probability distribution for three stations. The first column represents raw data, and the second column shows station detection probability. Each pair of plots corresponds to a station, with station names and scores indicated on the left.

As shown in Figure 7, the high-value detection probability areas expand with increasing magnitude. For magnitude 0.3, high detection probability areas are concentrated on the eastern side of the study area. For magnitude 1.5, the area of certain detection covers almost the entire study region. In the third column of Figure 7, for lower magnitudes, *P*(PMC) is higher than *P*(EMR) in areas with good monitoring capabilities, while *P*(PMC) is lower than *P*(EMR) in areas with worse monitoring capabilities. The differences between *P*(PMC) and *P*(EMR) decrease with increasing magnitude. At magnitudes above 0.5, the discrepancy is concentrated in the northwestern part of the study area, where *P*(PMC) is generally higher than *P*(EMR). As the magnitude increases, the differences between the detection probabilities of the two methods diminish, with *P*(PMC) showing a faster rate of change with increasing magnitude.

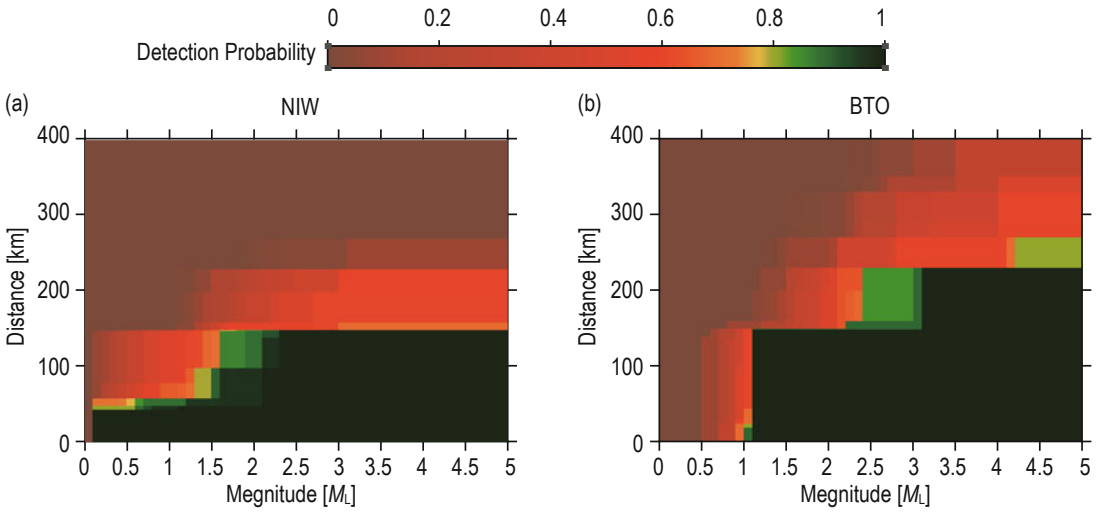

Figure 6 Stations exhibiting non-compliant decay patterns: distributions of detection probability with the station names labeled above each subplot.

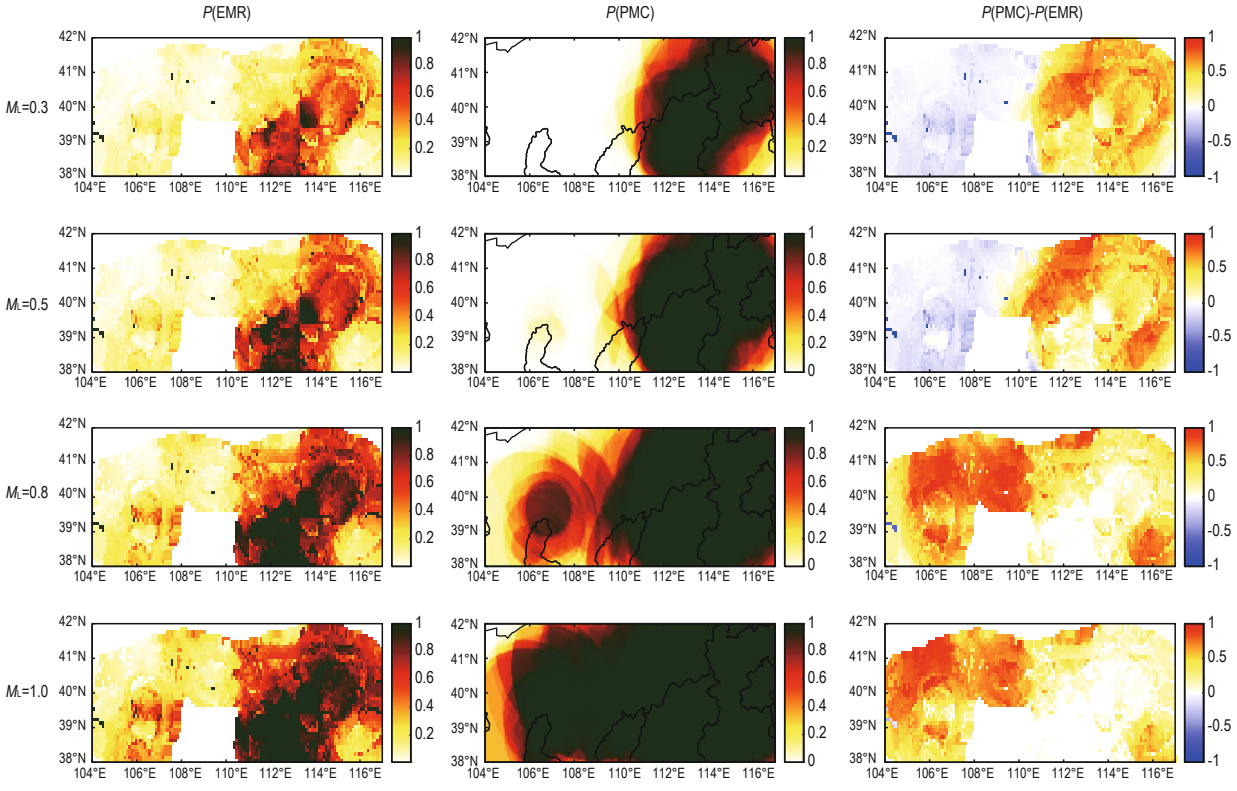

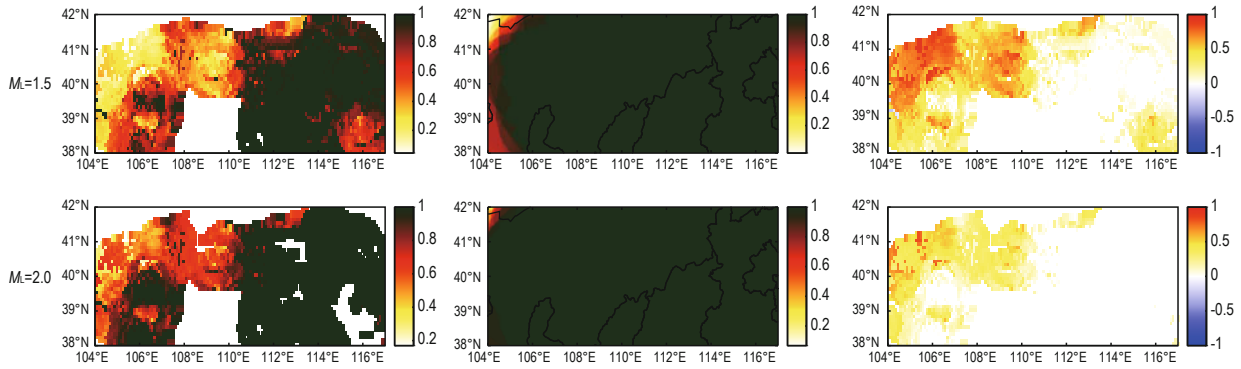

Figure 7. Spatial distribution of earthquake detection probability for different magnitude (0.3, 0.5, 0.8, 1.0, 1.5 and 2.0) using EMR method (first column) ,PMC method (second column) and the difference between the two methods (third column).

Figure 8 presents the completeness magnitudes (M_P and M_C(EMR)) obtained via the PMC and EMR methods, as well as their differences (M_C(EMR) − M_P). The PMC method provided complete estimates for the study area, whereas the EMR method yielded results only for a portion of the area (blank areas in Figures 8(a) and 8(c) indicate regions where the calculation conditions were not met and no assessment was made). The results of the two methods are positively correlated, showing that the monitoring capabilities gradually decrease from east to west. The difference map (Figure 8(c)) shows that M_C(EMR) is higher than M_P on the eastern side of the study area, whereas M_P is higher than M_C(EMR) in most of the central and western areas. Figure 9(a) displays the relationship between M_P and M_C(EMR) in the common calculable area, showing a positive and approximately linear correlation between the two. The dashed line represents the reference line (M_P = M_C(EMR)), with M_P being about 0.5 lower than M_C(EMR), indicating a systematic difference. Figure 9(b) shows that M_C(EMR) and the difference (M_C(EMR) − M_P) are positively correlated, suggesting that M_P is underestimated to a greater extent in areas with weaker monitoring capabilities. This was attributed to the overestimation of detection probability for lower magnitudes and areas with weak monitoring capabilities, as previously discussed. The higher M_C(EMR) values compared to M_P in the southern part of the study area were attributed to the truncation effect of data selection. In the PMC method, we did not consider the effects of

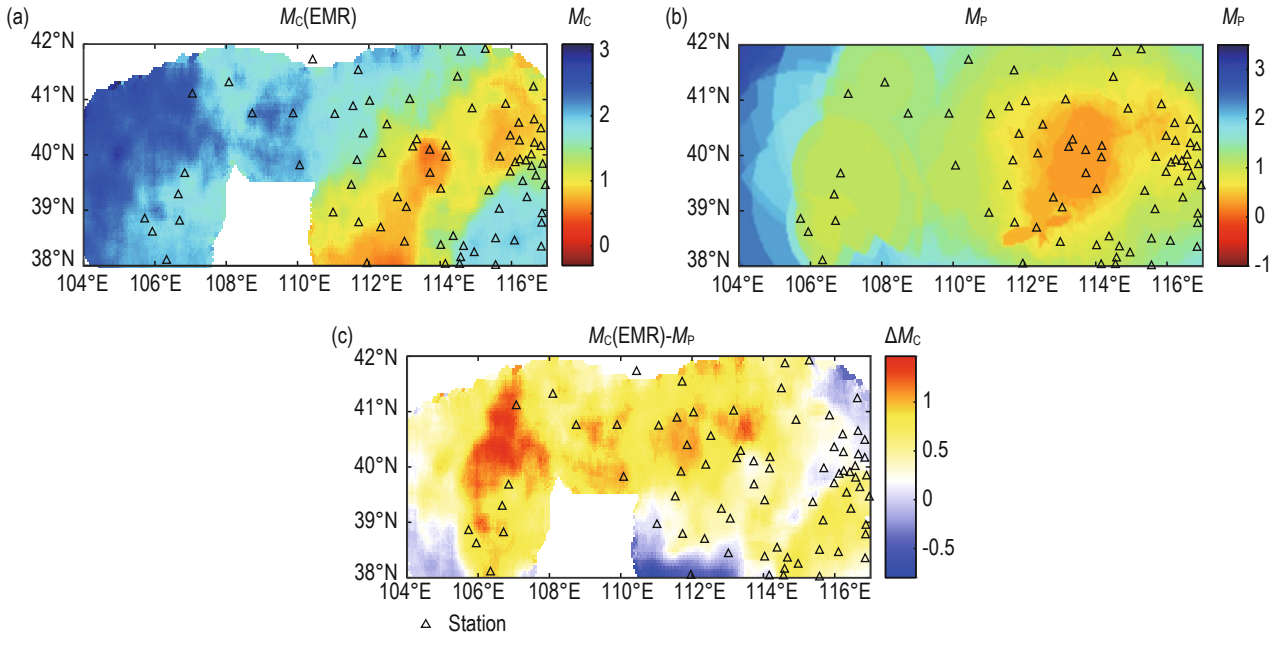

Figure 8. Comprehensive magnitude completeness: (a) M_C (EMR); (b) M_P; (c) M_C (EMR)−M_P.

stations and data outside the study area on the evaluation results, whereas the results of the EMR method, which employs actual observed data, are not affected by data truncation. A significant spatial heterogeneity in monitoring capabilities is observed within the study area, which is closely related to station distribution. The monitoring capabilities are better on the eastern side of the study area, with M_P below 1, whereas areas with dense station distribution in the northeast show M_P values below 0.5. The monitoring capabilities are the weakest in the western side of the study area, with M_P around 3. In areas with better monitoring capabilities, the assessment results of the two methods are closer, whereas in areas with weaker monitoring capabilities, M_P is lower than M_C (EMR). Evaluations performed using the EMR and PMC methods for the study area a decade earlier (Liu et al., 2013; Liu et al., 2014) showed higher M_C (EMR) and M_P, indicating that monitoring capabilities in the study area improved over the past decade.

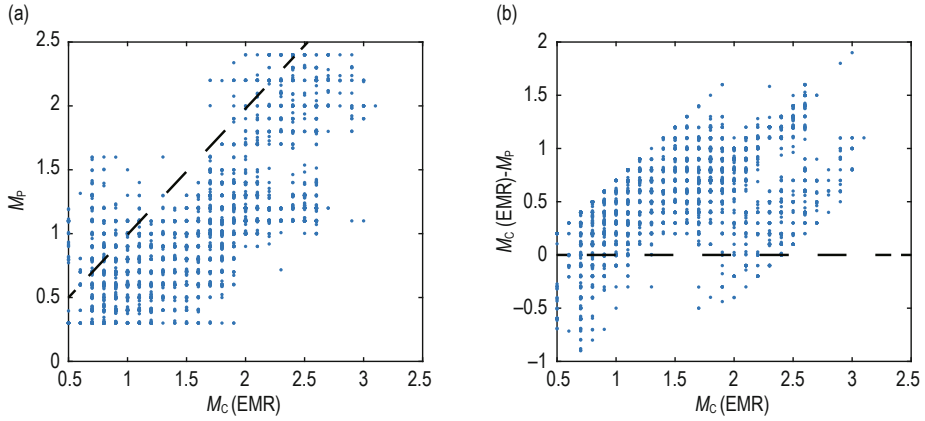

Figure 9. Relationship between the results of the two methods: (a) M_P vs. M_C (EMR); (b) M_C (EMR)−M_P vs, M_C (EMR).

Discussion

Calculations of detection probability require knowing the number of actual recorded earthquakes and the number of earthquakes that truly occurred. However, the true number of earthquakes is unknown. Therefore, the main challenge in evaluating detection probabilities lies in estimating the true number of earthquakes. The two methods used herein differ primarily in their approach to the estimation of the true number of earthquakes. In the PMC method, the network's earthquake catalog is used as a representation of true earthquake occurrences. Because of the inherent incompleteness of network catalogs, this approach may underestimate the detection probability. At the same time, in the EMR method, the number of actual earthquakes at lower magnitudes is extrapolated based on the Gutenberg–Richter relationship. This method is highly sensitive to the *b*-value so that even small errors can significantly impact the estimated true earthquake count. The discrepancies in completeness magnitudes obtained through these two methods reveal that in regions with weaker monitoring capabilities, the PMC method yields higher probabilities than the EMR method, supporting our hypothesis. Conversely, in regions with better monitoring capabilities, the differences between the results of the two methods are less pronounced.

We plotted the detection probability curves with respect to magnitude for nine grid points at different locations within the study area (Figure 10). The shapes of the curves, showing the relationship between detection probability and magnitude, vary between the two methods across different regions. In regions with robust monitoring capabilities (Figures 10(e)–(i)), the curves derived via both methods are in good agreement. However, in regions with weaker monitoring capabilities (Figures 10(a)–(d)), the curve of the PMC method deviates from the horizontal line (where the x-coordinate equals 1) at lower magnitudes compared to the EMR method. Notably, across all grid points, the curves generated using the PMC method exhibit a more rapid decay.

To investigate the effect of the distance for which station-wise detection probability is calculated on the network catalog completeness, two distance thresholds (D) were tested. Figure 11(a) presents the results for D = 400 km, and Figure 11(b) exhibits the results for D =

200 km. The difference (ΔM_P) between the two results is shown in Figure11(d) and (f). The two results are highly consistent, with minor discrepancies observed in regions with high network density. The distance to the fourth nearest station (D_{4th}) was selected as an indicator of network density (Density) to analyze its impact on the results, following Mignan et al. (2011) (Figure 11(c)). Lower D_{4th} values indicate higher network density. Figure 11(f) shows the variation in ΔM_P with D_{4th}, indicating a positive correlation between the two. Overall, ΔM_P is predominantly within 0.5, and for D_{4th} within 100 km, ΔM_P is mostly below 0.3. In regions where D_{4th} is less than 50 km, the results are very close, indicating that in densely populated station areas, M_P is primarily affected by nearby stations, whereas in sparsely populated areas, it is influenced more by distant stations. Figure 11(e) shows M_C (EMR), M_P, and M_C (EMR)−M_P as functions of D_{4th}. M_C (EMR) values are higher than M_P, and both M_C (EMR) and M_P are positively correlated with D_{4th} but show a notable degree of dispersion. This suggests that factors beyond station density also contribute to monitoring capabilities.

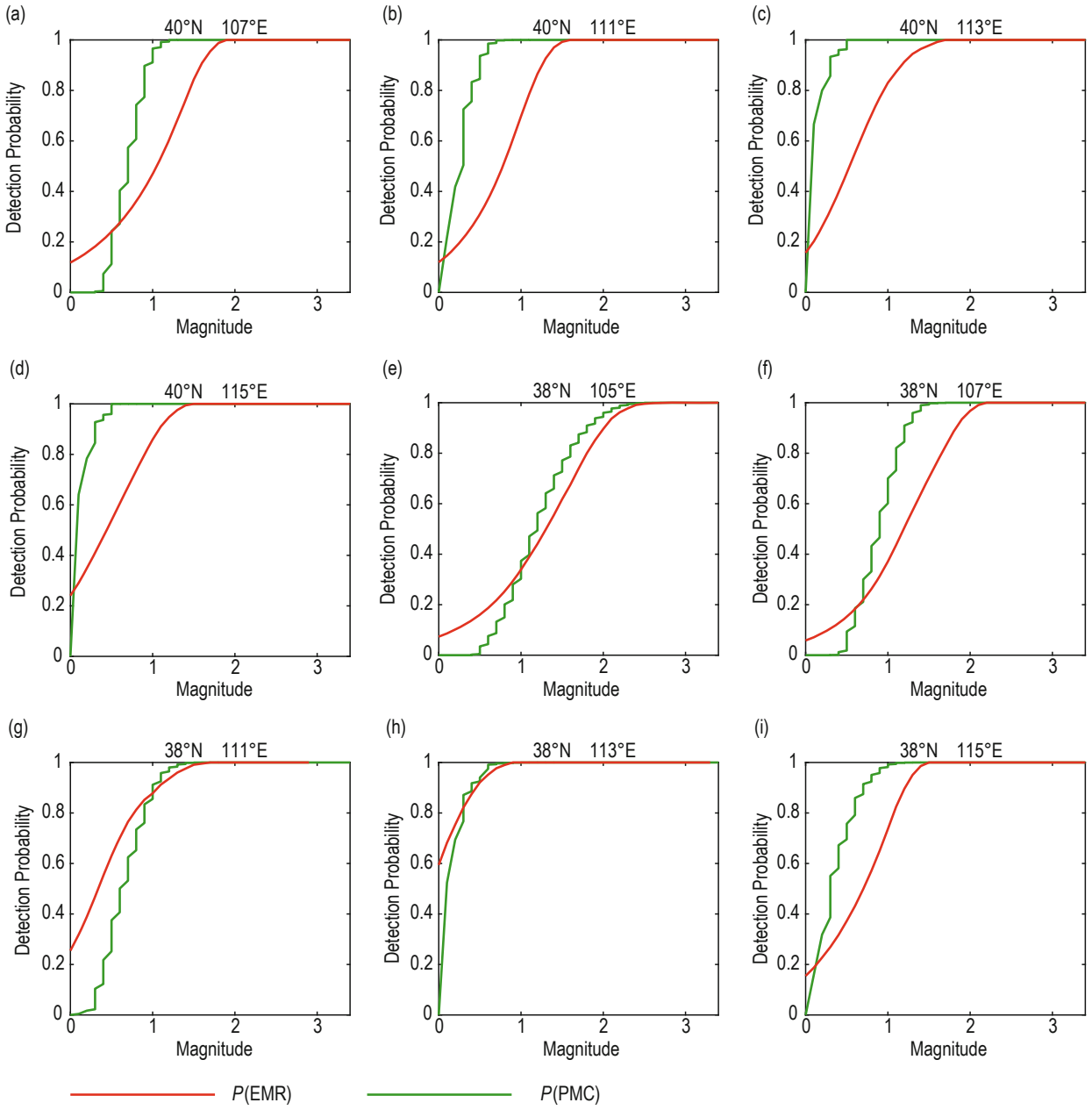

Figure 10 Decay curves of detection probability at different grid points.
The graph compares the detection probability curves for 9 points, with each subplot representing one point. Latitude and longitude are labeled above each subplot.

Figure 12 exhibits the changes in P(EMR) and P(PMC) with D_{4th} and magnitude. Both P(EMR) and P(PMC) are negatively correlated with D_{4th} and positively correlated with magnitude, with P(PMC) showing a more pronounced variation with D_{4th} and magnitude than P(EMR).

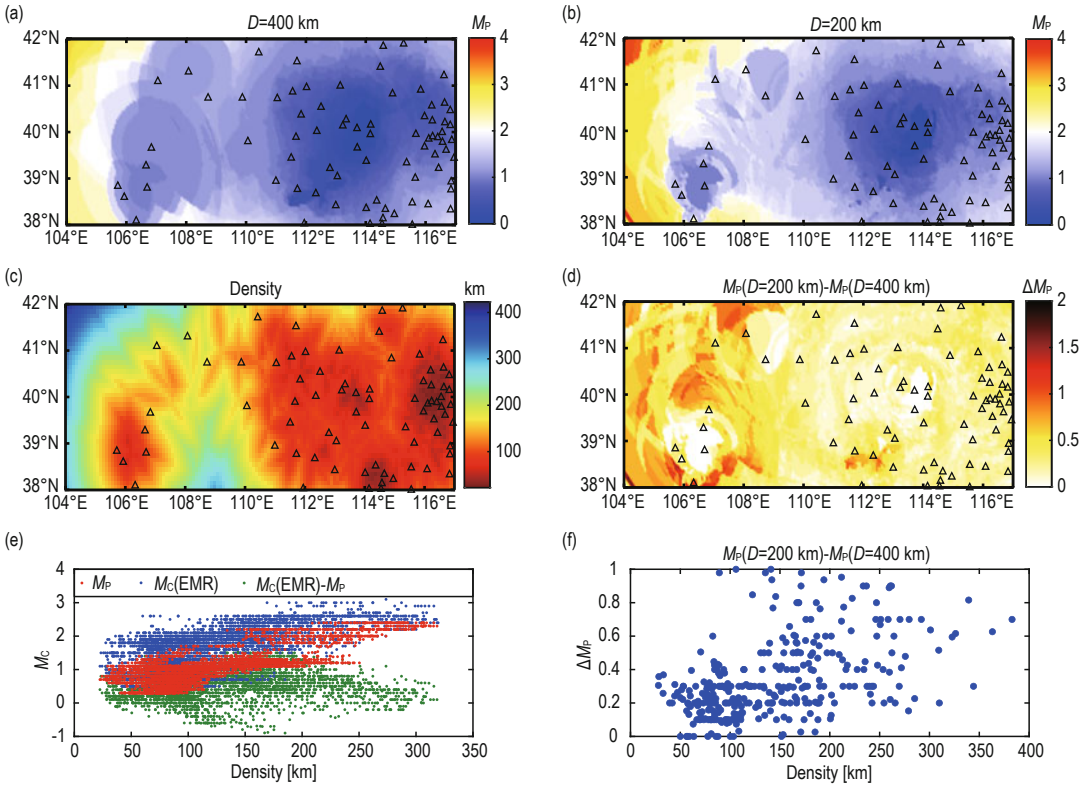

Figure 11. Effects of parameters used in station-wise evaluation as well as network density on results. (a) Distribution of M_P for a station evaluation range of 0–400 km; (b) distribution of M_P for a station evaluation range of 0–200 km; (c) distribution of network density parameter D_{4th}; (d) difference between the results for the two evaluation ranges; (e) M_C (EMR), M_P, and M_C (EMR)−M_P as functions of D_{4th}; (f) relationship between ΔM_P and D_{4th}.

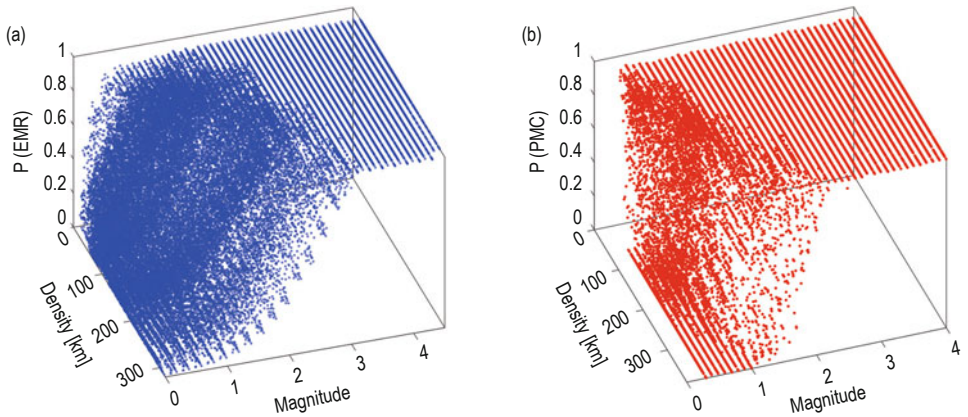

Figure 12. Variation in the detection probability of the network with magnitude and network density (a) P(EMR); (b) P(PMC).

Schorlemmer and Woessner (2008) compared the PMC and EMR methods in Southern California and reported that M_P is lower than M_C (EMR) at 77% of the grid points and higher at approximately 11%. Conversely, assessments in Switzerland (Nanjo et al., 2010) and seismic array studies (Jiang et al., 2015) have shown that M_P is generally higher than M_C (EMR). Herein, M_C (PMC) is lower than M_C (EMR), aligning

with the results of the Southern California study but with a more pronounced difference. Figure 8 shows that M_C (EMR) is lower than M_P at the edges of the study area. This discrepancy was attributed to data truncation effects arising from the exclusion of stations and data from outside the study area when assessing the monitoring capabilities within the study region. Two types of truncation effects could have affected our estimates of network monitoring capabilities. First, relying solely on earthquake data from within the study area might not fully reflect the detection capabilities of stations located near its edges because, in this case, events recorded by these stations outside the region are omitted (Li and Huang, 2014). However, herein, data solely from within the study area was used to better reflect each station's ability to record earthquakes in that region. Thus, we did not expand our dataset. The second truncation effect concerns station selection, potentially leading to the underestimation of monitoring capabilities, particularly in the southern part of the study area.

The EMR method shows commendable reliability and stability compared with other methods (Woessner and Wiemer, 2005), especially for small sample sizes (Zhou et al., 2018). However, it is prone to overestimation (Pavlenko et al., 2022) and fails to provide assessments in regions with insufficient data. PMC methodically assesses M_C by analyzing the characteristics of the seismic network without assuming a G–R model. This method uses actual earthquake observations to overcome the "blank areas" caused by a scarcity of earthquakes, thereby providing comprehensive evaluations across the study area. However, the PMC method operates under the assumption that the network's earthquake record is complete. This assumption is then used to assess station detection probabilities, which are further used to derive network detection probabilities and completeness magnitude. This process is based on circular reasoning, making PMC inherently inconsistent. Thus, PMC's evaluation lower limit is the seismic network's actual M_C. Therefore, when using PMC, it is essential to ensure that its underlying assumptions are met or to correct biases by combining PMC with methods such as EMR based on prior information.

Conclusion

The completeness of the earthquake catalogs often shows temporal and spatial heterogeneity. At the same time, detection probability provides a more detailed description of the earthquake catalog. Herein, the northern margin of the Ordos Block was selected as the study area to evaluate the overall temporal changes in the completeness of the earthquake catalog since 1965. The PMC and EMR methods were used to analyze the earthquake catalog since 2010 to obtain the detection probability and completeness magnitude in the study area. The results of the two methods were compared, with the main findings presented below:

(1) Using the magnitude–rank method and the MAXC method, we studied the temporal changes in the completeness of the earthquake catalog from 1965 to June 2023. M_C in the study area showed a phased decline, stabilizing after 2010, which was attributed to the improvement of monitoring capabilities and the increase in the density of seismic networks. At the same time, significant differences in M_C were observed across different periods.

(2) The PMC method was used to obtain the distribution of detection probability in the distance–magnitude space for 76 stations, along with station scores for the period from 2010 to June 2023. The detection capabilities of different stations significantly differed. According to the calculation principles and actual results, station detection probability is affected by the completeness of the network catalog, potentially leading to overestimation at lower magnitudes. The obtained M_P and M_C (EMR) supported these speculations.

(3) We used the PMC and EMR methods to obtain detection probabilities at different grid points in the study area (P(PMC) and P(EMR)). In areas with weaker monitoring capabilities, P(PMC) was lower than P(EMR), with the difference decreasing with the increase in magnitude. The curves of P(PMC) and P(EMR) versus magnitude were consistent in areas with good monitoring capabilities. At the same time, in areas with poor monitoring capabilities, the P(PMC) curve deviated from the horizontal line at lower magnitudes compared to P(EMR). Additionally, P(PMC) varied more significantly with the changes in network density and magnitude.

(4) The detection probabilities (M_P and M_C (EMR)) at different grid points in the study area were positively correlated and exhibited an approximately linear relationship. M_P was generally lower than M_C (EMR), with a systematic difference of about 0.5. The underestimation of M_P was related to the overestimation

of station-wise detection probabilities, which was more significant in areas with weaker monitoring capabilities. The statistical range of station-wise detection probabilities affected the M_P results, especially in sparsely populated areas.

(5) The distribution of monitoring capabilities of the seismic network along the northern margin of the Ordos Block was uneven. The obtained M_C values increased with decreasing station density. In the eastern part of the study area, M_P was less than 1, and in the densely populated northeastern region, M_P could be less than 0.5. The western part of the study area showed the worst monitoring capabilities, with M_P around 3. Data and station selection affected the assessment results at the edges of the study area.

Acknowledgments

This work was supported by the Director Fund of the Inner Mongolia Autonomous Region Seismological Bureau (No. 2023GG02, 2023MS05) and the Inner Mongolia Natural Science Foundation General Project (No. 2024MS04021). The study utilized the National Unified Official Catalogue provided by the China Earthquake Networks Center.

References

Amorese, D., 2007, Applying a change-point detection method on frequency-magnitude distributions: Bulletin of the Seismological Society of America, **97**(5), 1742–1749.

Bi, J. M., Song, C., Cao, F. Y., 2023, Activity characteristics of significant earthquake swarms in the Bohai Rim region: Applied Geophysics, **20**(1), 100–115.

Cao, A., Gao, S.S., 2002, Temporal variation of seismic b-values beneath northeastern Japan island arc: Geophysical Research Letters, **29**(9), 48–41–48–43.

Conover, W. J. ,1999, Practical nonparametric statistics: John Wiley & Sons.

D'Alessandro, A., Luzio, D., D'Anna, G., et al., 2011, Seismic Network Evaluation through Simulation: An Application to the Italian National Seismic Network: Bulletin of the Seismological Society of America, **101**(3):1213–1232.

Gao, L. X., Hou, D., Li, J., et al., 2016, Movement characteristics and present seismic activity of Ordos Block: Geodesy and Geodynamics, **7**(6): 451–458.

Goertz-Allmann, B. P., Wiemer, S., 2013 , Geomechanical modeling of induced seismicity source parameters and implications for seismic hazard assessment: Geophysics, **78**(1), KS25–KS39.

Gomberg, J., Seismicity and detection/location threshold in the southern Great Basin seismic network: Journal of Geophysical Research: Solid Earth, 1991, **96**(B10): 16401–16414.

Gong, W. C., Chen, H. Y., Gao, Y. J., et al., 2024, A test on methods for M_C estimation and spatial-temporal distribution of *b*-value in the eastern Tibetan Plateau: Frontiers in Earth Science, **12**, 1335938.

Gutenberg, B., Richter, C. F., 1944, Frequency of earthquakes in California: Bulletin of the Seismological Society of America, **34**(4), 185–188.

Hainzl, S., 2016, Rate-dependent incompleteness of earthquake catalogs: Seismological Research Letters, **87**(2A): 337–344.

Hainzl, S., 2022, ETAS-approach accounting for short-term incompleteness of earthquake catalogs: Bulletin of the Seismological Society of America, **112**(1), 494–507.

Huang, Y. L., Zhou, S. Y., Zhuang, J. C., 2016. Numerical tests on catalog-based methods to estimate magnitude of completeness: Chinese Journal of Geophysics (in Chinese), **59**(4), 1350–1358.

Jiang, C. S., Fang, L. H., Han, L. B., et al., 2015. Assessment of earthquake detection capability for the seismic array: A case study of the Xichang seismic array: Chinese Journal of Geophysics (in Chinese), **58**(3), 832–843.

Jiang, C. S., Wu, Z. L., 2011. Intermediate-term medium-range Accelerating Moment Release (AMR) priori to the 2010 Yushu M_S7.1 earthquake: Chinese Journal of Geophysics (in Chinese), **54**(6), 1501–1510.

Kagan, Y. Y., 2004, Short-term properties of earthquake catalogs and models of earthquake source, Bulletin of the Seismological Society of America, **94**(4), 1207–1228.

Kværna, T., Ringdal, F., 1999, Seismic threshold monitoring for continuous assessment of global detection capability: Bulletin of the Seismological Society of America, **89**(4): 946–959.

Leptokaropoulos, K. M., Adamaki, A. K., Roberts, R. G., et al., 2018, Impact of magnitude uncertainties on seismic catalogue properties: Geophysical Journal

International, **213**(2), 940–951.

Li, Z. C., Huang, Q. H., 2014. Assessment of detectability of the Capital-circle Seismic Network by using the probability-based magnitude of completeness (PMC) method: Chinese Journal of Geophysics (in Chinese), **57**(8), 2584–2593.

Liu, F., Jiang, C. S., Zhang, F., et al., 2013. Monitoring capacity of seismic network in Inner Mongolia region based on EMR method: Earth Science(in Chinese), **38**(6), 1356–1362.

Liu, F., Jiang, C. S., Zhang, F., et al., 2014. A study on detection capability of the Inner Mongolia regional seismic network: Acta Seismologica Sinica(in Chinese), **36**(5), 919–929.

Liu, R. F., Gao, J. C., Chen, Y. T., et al., 2008, Construction and development of digital seismograph networks in China:Earthquake Science **21**(5), 535–541.

Lombardi, A. M., 2021, A normalized distance test for co-determining the completeness magnitude and *b*-value of earthquake catalogs: Journal of Geophysical Research: Solid Earth, **126**(3), e2020JB021242.

Martinsson, J., Jonsson, A., 2018, A new model for the distribution of observable earthquake magnitudes and applications to *b*-value estimation: IEEE Geoscience and Remote Sensing Letters, **15**(6), 833–837.

Mignan, A., Jiang, C. S., Zechar, J. D., et al., 2013, Completeness of the Mainland China Earthquake Catalog and Implications for the Setup of the China Earthquake Forecast Testing Center: Bulletin of the Seismological Society of America, **103**(2A):845–859.

Mignan, A., Werner, M. J., Wiemer, S., et al., 2011, Bayesian Estimation of the Spatially Varying Completeness Magnitude of Earthquake Catalogs: Bulletin of the Seismological Society of America, **101**(3), 1371–1385.

Mignan, A., Woessner, J. ,2012, Theme IV—understanding seismicity catalogs and their problems: Community online resource for statistical seismicity analysis.

Mizrahi, L., Nandan, S., Wiemer, S., 2021, Embracing data incompleteness for better earthquake forecasting: Journal of Geophysical Research: Solid Earth, **126**(12), e2021JB022379.

Nanjo, K. Z., Schorlemmer, D., Woessner, J., et al., 2010, Earthquake detection capability of the Swiss Seismic Network: Geophysical Journal International, **181**(3), 1713–1724.

Omi, T., Ogata, Y., Hirata, Y., et al., 2014, Estimating the ETAS model from an early aftershock sequence: Geophysical Research Letters, **41**(3), 850–857.

Pavlenko, V. A., Zavyalov, A.D., 2022, Comparative analysis of the methods for estimating the magnitude of completeness of earthquake catalogs, Izvestiya: Physics of the Solid Earth, **58**(1), 89–105.

Ram, K. T., Harihar, P., Daya, S., 2022, Spatio-temporal distribution of earthquake occurrence in Eastern Himalaya and vicinity (26° N–31° N and 87° E–98° E) based on b-value and fractal dimension: Applied Geophysics, **19**(3), 458–469.

Rydelek, P. A., Sacks, I. S., 1989, Testing the completeness of earthquake catalogues and the hypothesis of self-similarity: Nature, **337**(6204), 251–253.

Schorlemmer, D., Hirata, N., Ishigaki, Y., et al., 2018, Earthquake detection probabilities in Japan: Bulletin of the Seismological Society of America, **108**(2), 702–717.

Schorlemmer, D., Woessner, J., 2008, Probability of Detecting an Earthquake: Bulletin of the Seismological Society of America, **98**(5), 2103–2117.

Wang, Y. W., Jiang, C. S., Liu, F., et al., 2017. Assessment of earthquake monitoring capability and score of seismic station detection capability in China Seismic Network (2008—2015): Chinese Journal of Geophysics (in Chinese), **60**(7), 2767–2778.

Wiemer, S., Wyss, M., 2000, Minimum magnitude of completeness in earthquake catalogs: Examples from Alaska, the western United States, and Japan: Bulletin of the Seismological Society of America, **90**(4), 859–869.

Woessner, J., Wiemer, S., 2005, Assessing the Quality of Earthquake Catalogues: Estimating the Magnitude of Completeness and Its Uncertainty: Bulletin of the Seismological Society of America, **95**(2), 684–698.

Xu, X. W., Wu, X. Y., Yu, G. H., et al., 2017. Seismo-geological signatures for identifying M≥7.0 earthquake risk areas and their preliminary application in mainland China: Seismology and Geology(in Chinese), **39**(2), 219–275.

Zhou, Y. J., Zhou, S. Y., Zhuang, J. C., 2018, A test on methods for M_C estimation based on earthquake catalog: Earth and Planetary Physics, **2**(2), 150–162.

Zhuang, J. C., 2011, Next-day earthquake forecasts for the Japan region generated by the ETAS model: Earth, Planets and Space, **63**(3), 207–216.

Zúñiga, F. R., Wyss, M., 1995, Inadvertent changes in magnitude reported in earthquake catalogs: Their evaluation through b-value estimates: Bulletin of the Seismological Society of America, **85**(6): 1858–1866.

Zhang Fan received his Master's degree in Statistics from Inner Mongolia University of Finance and Economics in 2014. He is currently employed at the Inner Mongolia Seismic Station of the Inner Mongolia Autonomous Region Seismological Bureau. Since September 2019, he has been pursuing a Ph.D. at the School of Control and Computer Engineering at North China Electric Power University. His main research interests include earthquake prediction and machine learning.